Microelectronic Engineering 226 (2020) 111289

Contents lists available at ScienceDirect

Microelectronic Engineering

journal homepage: www.elsevier.com/locate/mee

Research paper

μ-Coriolis mass flow sensor with improved flow sensitivity through modelling of the sensor

T.V.P. Schut[a,*], R.J. Wiegerink[a], J.C. Lötters[a,b]

[a] MESA + Institute for Nanotechnology, University of Twente, Enschede, the Netherlands
[b] Bronkhorst High-Tech BV, Ruurlo, the Netherlands

ARTICLE INFO

Keywords:
Flow
Sensor
Model
Coriolis
FEM
Surface Channel
Optimization
Sensitivity

ABSTRACT

In this paper we present μ-Coriolis mass flow sensor devices with improved flow sensitivity. An FEM model is set up which can estimate various parameters of a μ-Coriolis device such as resonance frequency, spring constants and Coriolis forces. These parameters are then used in an analytical model to determine flow sensitivity. The presented FEM model allows for fast simulation of these properties, enabling optimization by varying many dimensions and other properties of the designs and see their influence on flow sensitivity. Three devices have been fabricated based on simulation results. All have been characterized and a comparison was made between different devices and between measurement and simulation results. The model predicts the resonance frequencies with less than 10% error for all except 1 (out of 6) devices. The predicted sensitivities are within 6–40% accurate depending on the type of device. Flow sensitivity is improved approximately 4–11 times with respect to a reference device of typical dimensions.

1. Introduction

A Coriolis mass flow sensor measures true mass flow, independent of fluid properties such as density and viscosity. This has made them of great importance in the field of mass flow measurement [1,2]. In the area of micro-machined flow sensors, thermal sensors are still widely used for their high resolution [3,4]. Haneveld et al. presented a highly sensitive μ-Coriolis mass flow sensor [5], making the first step towards reaching the resolution of thermal flow sensors. Improvements have been made upon this sensor, which resulted in a more sensitive μ-Coriolis presented by Groenesteijn et al. [6]. It had a zero-flow stability 40 times better than state of the art at that time. Alveringh et al. showed that the resolution of the sensor in [6] can still be improved by a factor of 50 before reaching the fundamental limit associated with random thermal motion of the vibrating channel [7]. This can be done in several ways, e.g. by improving the sensitivity of the capacitive readout [6,8]. Another option is increasing the signal-to-noise ratio in the readout electronics as well as in the mechanical design of the sensor [9,10]. The focus of the research presented in this paper lies on improving the mechanical design to achieve a higher flow sensitivity and resolution.

2. Materials & methods

2.1. Operating principle

A Coriolis mass flow sensor measures true mass flow independent from fluid properties such as density and viscosity. Fig. 1 shows the operation principle of a μ-Coriolis mass flow sensor. The sensor consists of a rectangular channel loop. The channel is fixed at the in−/outlet channel sections, as depicted in the figure. The channel loop is brought into resonance by Lorentz forces. These Lorentz forces are generated by a magnetic field **B** and an alternating current i flowing through a metal track on top of the micro-channel. This actuates the sensor in the *Twist*/actuation mode with actuation angle θ_a. When a fluid flows through the micro-channel with a mass flow rate ϕ_m, Coriolis forces are induced in the channel section as indicated in Fig. 1b. This causes additional vibration in the *Swing*/detection mode with an angle θ_d and displacement Δz_d.

* Corresponding author.
E-mail address: T.V.P.Schut@utwente.nl (T.V.P. Schut).

https://doi.org/10.1016/j.mee.2020.111289
Received 9 December 2019; Received in revised form 13 March 2020; Accepted 14 March 2020
Available online 17 March 2020
0167-9317/ © 2020 Elsevier B.V. All rights reserved.

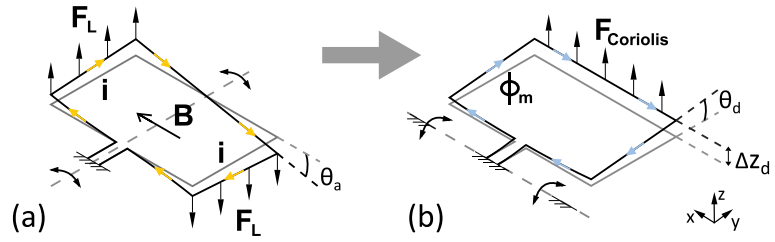

Fig. 1. Operation principle of a μ-Coriolis mass flow sensor. (a): The channel is brought into resonance in the *Twist* mode through Lorentz force F_L resulting from magnetic field **B** and alternating current *i*. (b): A mass flow ϕ_m through the channel induces vibration in the *Swing* mode through Coriolis force $F_{Coriolis}$.

2.2. Analytical model

A model has been set up which can be used to approximate the sensitivity of a μ-Coriolis mass flow sensor. Sensitivity to flow is quantified as the ratio between the detection and actuation angles (θ_d/θ_a) per mass flow rate ϕ_m (see Fig. 1). In the model, any dimensions of the mechanical design can be varied and their influence on the sensitivity of the sensor can be investigated. Groenesteijn et al. previously presented a similar model based on Matlab's SPACAR package [11]. The model presented in this paper is based on a FEM simulation (COMSOL Multiphysics) in combination with an analytical model of the sensor.

Haneveld et al. [5] derived an analytical model describing flow sensitivity of a Coriolis mass flow sensor. They assumed that the actuation and detection resonance frequencies (ω_a and ω_d respectively) are far apart such that the final equation can be simplified. However, this is not always true. Especially when simulating many different sets of dimensions, the resonance frequencies can be very close in value. Therefore, the flow sensitivity needs to be derived without making the assumption that $\omega_a \gg \omega_d$ or $\omega_a \ll \omega_d$.

Vibration of the sensor can be described by a second order differential equation. [5]:

$$J_{a,d}\frac{d^2\theta_{a,d}(t)}{dt^2} + R_{a,d}\frac{d\theta_{a,d}(t)}{dt} + S_{a,d}\theta_{a,d}(t) = \tau_{a,d}(t) \tag{1}$$

Where the subscript a,d indicates either actuation or detection mode vibration. $J_{a,d}$ is the moment of inertia, $R_{a,d}$ is the damping coefficient, $S_{a,d}$ is the torsional spring constant, $\theta_{a,d}$ is the angular displacement and finally $\tau_{a,d}$ is the actuation torque or detection torque induced by Coriolis forces.

The Coriolis force in a section of channel with length L rotating with an angular velocity $d\theta/dt$ can be expressed as:

$$F_C = -2L\phi_m\frac{d\theta}{dt} \tag{2}$$

Where ϕ_m is the mass flow rate through the channel. Each channel section has its own rotation angle θ, dependent on the actuation angle θ_a. The total Coriolis force on the channel induces a detection torque $\tau_d(t)$ proportional to the actuation angular velocity $d\theta_a/dt$:

$$\tau_d \propto \frac{d\theta_a}{dt} \tag{3}$$

The actuation angle $\theta_a(t)$ will be a sinusoidal signal resulting from Lorentz forces bringing the sensor loop into resonance:

$$F_L(t) = B{\cdot}L_y{\cdot}\hat{i}_{act}\cos(\omega_a t) \tag{4}$$

$$\tau_a(t) = F_L{\cdot}L_x \tag{5}$$

Where L_x and L_y are the length of the sensor loop in the x and y direction respectively. The resulting actuation angle and angular velocity will be of the form:

$$\theta_a(t) = \alpha\sin(\omega_a t) \tag{6}$$

$$\frac{d\theta_a(t)}{dt} = \omega_a{\cdot}\alpha\cos(\omega_a t) \tag{7}$$

From Eq. (3) it then follows that $\tau_d(t)$ is of the same form as $d\theta_a/dt$:

$$\tau_d(t) = T_d\cos(\omega_a t) \tag{8}$$

Where T_d is the amplitude of $\tau_d(t)$, being linearly dependent on ω_a, α and ϕ_m. Applying $\tau_d(t)$ to Eq. (1) gives a detection angle of the following form:

$$\theta_d(t) = \beta\sin(\omega_a t) + \gamma\cos(\omega_a t) \tag{9}$$

Inserting this in Eq. (1) and solving for β and γ gives:

$$\beta = \gamma\frac{\omega_a\omega_d}{(\omega_d^2-\omega_a^2)Q_d} \tag{10}$$

$$\gamma = \frac{T_d\omega_d^2Q_d^2(\omega_d^2-\omega_a^2)}{S_d(Q_d^2(\omega_d^2-\omega_a^2)^2+\omega_a^2\omega_d^2)} \tag{11}$$

Where Q_d is the detection mode quality factor. Now that we have obtained expressions for γ and β, we can derive the ratio between the actuation and detection angle amplitudes:

$$\theta_d(t) = \beta\sin(\omega_a t) + \gamma\cos(\omega_a t) = \sqrt{\beta^2+\gamma^2}{\cdot}\sin\left(\omega_a t + \arctan\left(\frac{\gamma}{\beta}\right)\right) \tag{12}$$

$$\frac{\hat{\theta}_d}{\hat{\theta}_a} = \frac{\sqrt{\beta^2+\gamma^2}}{\alpha} \tag{13}$$

With Eqs. (10) and (11) this gives:

$$\frac{\hat{\theta}_d}{\hat{\theta}_a} = \frac{T_d\omega_d^2Q_d^2(\omega_d^2-\omega_a^2)}{\alpha S_d(Q_d^2(\omega_d^2-\omega_a^2)^2+\omega_a^2\omega_d^2)}\sqrt{1+\frac{\omega_a\omega_d}{(\omega_d^2-\omega_a^2)Q_d}} \tag{14}$$

Since what is finally measured is the displacement of the channel in the z direction Δz_d (see Fig. 1), the flow sensitivity is finally quantified as:

$$\frac{\hat{\Delta}z_d}{\hat{\theta}_a} = L_y{\cdot}\frac{\hat{\theta}_d}{\hat{\theta}_a} \tag{15}$$

$$\frac{\hat{\Delta}z_d}{\hat{\theta}_a} = \frac{L_yT_d\omega_d^2Q_d^2(\omega_d^2-\omega_a^2)}{\alpha S_d(Q_d^2(\omega_d^2-\omega_a^2)^2+\omega_a^2\omega_d^2)}\sqrt{1+\frac{\omega_a\omega_d}{(\omega_d^2-\omega_a^2)Q_d}} \tag{16}$$

Where L_y is the distance between the detection mode rotational axis and the channel section where $\hat{\Delta}z_d$ is measured (Further on displayed in Fig. 2b). Eq. (15) holds for small angles θ_d. From Eq. (16), it seems as if L_x has no influence on the sensitivity. However, the detection torque T_d is directly dependent on L_x and other parameters (ω_a, ω_d, S_d and Q_d) are affected by L_x as well.

2.3. FEM model

A schematic representation of the FEM model is depicted in Fig. 2. The FEM model consists of two simulation steps. Firstly, a 2D simulation step of the channel cross-section (Fig. 2a) calculates mechanical

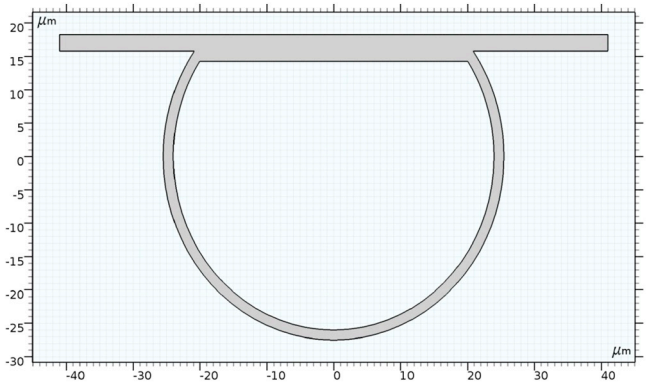

(a) Channel cross-section in COMSOL Multiphysics for 2D simulation step. This stationary step generates mechanical properties of the cross-section such as area, second moment of area and torsion constant.

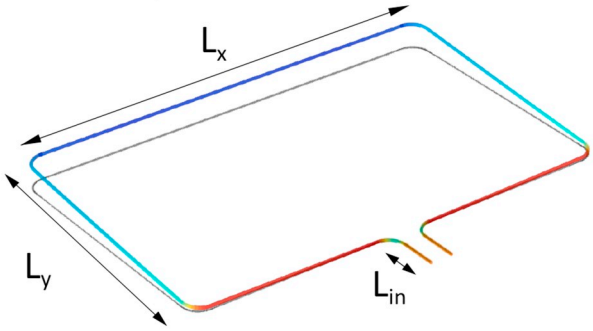

(b) Channel loop geometry in COMSOL Multiphysics for 3D eigenfrequency simulation step. Dimensions of interest are indicated in the figure. This step uses the resulting parameters from the previous 2D simulation step to generate parameters such as resonance frequencies and torsional spring constants of the resonator.

Fig. 2. Schematic representation of the 2-step FEM simulation of the sensor.

properties such as second moment of area and torsion constant. These are then used in a following 3D eigenfrequency simulation step (Fig. 2b). The 3D structure in Fig. 2b consists of a collection of 1D line elements in 3D space. This type of structure allows for very fast

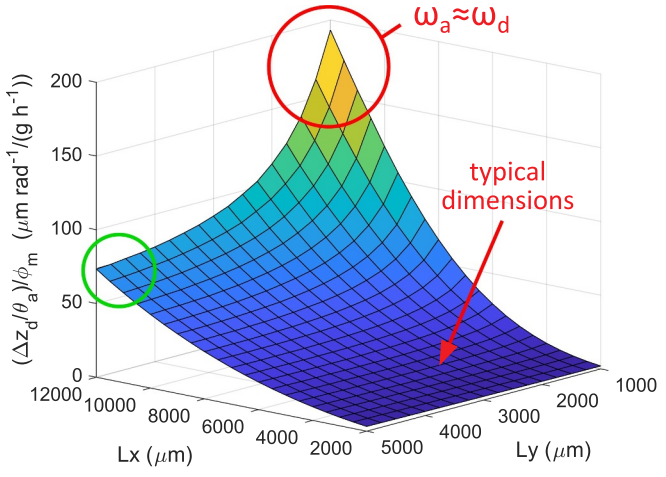

Fig. 3. Simulated flow sensitivity in relation to L_x and L_y (see Fig. 2). Large L_x and small L_y give a high sensitivity but low stability since ω_a and ω_d are close in value in this range. Small changes in ω_a/ω_d or Q_d can cause significant changes in flow sensitivity. Large L_x and L_y gives relatively high flow sensitivity and better stability.

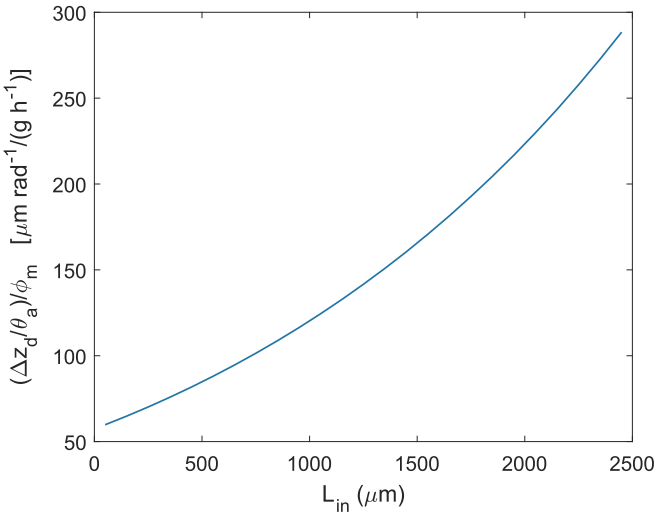

Fig. 4. Simulated flow sensitivity in relation to L_{in} (see Fig. 2). Larger L_{in} gives higher sensitivity.

simulation. Different cross-sectional geometries can be coupled to the various line elements to simulate the influence of e.g. spring suspensions or channel sections with different diameters. The 3D simulation step calculates the resonance frequencies and torsional spring constants of the two modes. Coriolis forces are calculated by evaluating Eq. (2) for each channel section. The total Coriolis/detection mode torque amplitude T_d is then derived. Additionally, ω_a, ω_d, α and S_d are calculated in the simulation. Combining these parameters with Eq. (16) and the measured quality factor Q_d gives the simulated flow sensitivity.

Simulating the aforementioned parameters for one set of dimensions can be done in around 30 s. Thus, many different dimensions and geometry designs can be compared relatively fast by sweeping variables. This way, the design of the sensor can be easily optimised to increase the flow sensitivity. Sweeps were done of many dimensions, such as channel diameter, wall thickness, loop size (L_x&L_y) and in−/outlet length (L_{in}). Although reducing the channel diameter as well as channel wall thickness do have a small positive effect on sensitivity, the first greatly increases pressure drop and the latter is already made as thin as the fabrication process allows. Therefore, these properties are not considered as practical design changes. In this paper, only the parameters L_x, L_y and L_{in} are considered. Fig. 3 shows the simulated flow sensitivity for a range of values of L_x and L_y. As can be seen from the figure, the highest sensitivity is found when L_x is large and L_y is small. However, this is also the range where the actuation and detection mode resonance frequencies are close in value. This is an unstable region, since a small change in Q_d or ω_a/ω_d can cause a significant change in flow sensitivity. For larger L_y, the resonance frequencies are further apart in value and the sensitivity is still relatively high (indicated in Fig. 3). Fig. 4 shows the simulated flow sensitivity in relation to L_{in}. When L_{in} increases, the flow sensitivity increases. The devices presented in this paper are based on these simulation results.

2.4. Fabrication & devices

The fabrication process of the sensor is based on the *Surface Channel Technology* (SCT) proposed in [12]. A simplified schematic representation of the fabrication process is displayed in Fig. 5. First, a layer of low-stress silicon-rich silicon nitride (SiRN, Thickness: 500 nm) is deposited on a Silicon wafer by Low-Pressure Chemical Vapour Deposition (LPCVD), see Fig. 5a. On top of this, a layer of silicon di-oxide (SiO_2) is deposited (LPCVD, Thickness: 500 nm), serving as a hard mask. Slits of 5 × 2 μm are etched through both layers by plasma etching, see Fig. 5b. Then the layer of SiO_2 is removed and a channel is formed by semi-

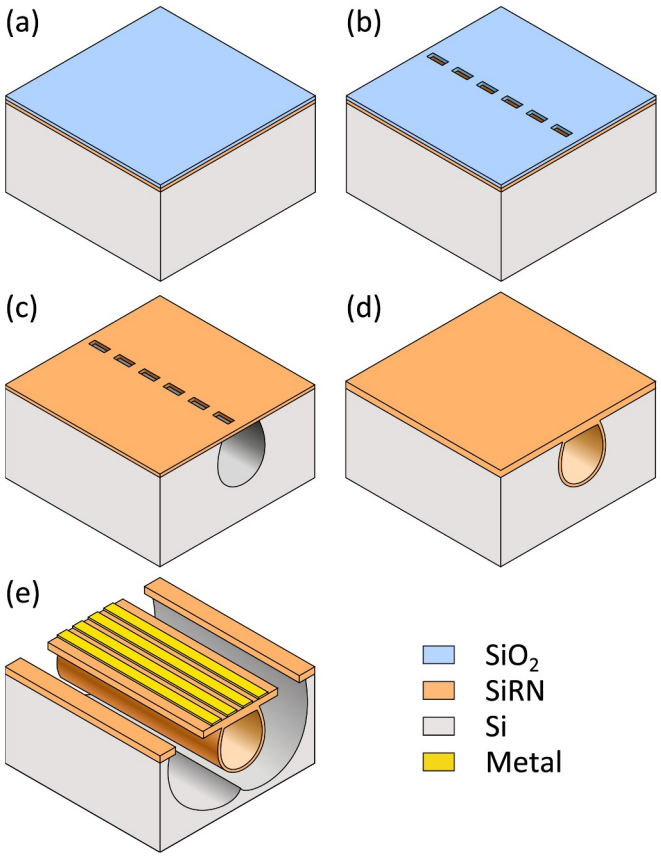

Fig. 5. Fabrication process for *Surface Channel Technology*. (a): Silicon wafer with 500 nm SiRN and 500 nm SiO_2. (b): Patterning of slit openings. (c): Removal of SiO_2 hard mask and forming of the surface channel. (d): Closing of the channel. (e): Patterning of metal and release of the channel.

isotropically etching silicon through the slits, see Fig. 5c. This is done by plasma etching as well. The channel is closed by conformally depositing another layer of low-stress SiRN, see Fig. 5d. Metal tracks are patterned on top the channel (Fig. 5e), these are used for actuation and readout of the sensor. Following this, openings are etched through the nitride and finally the channel is released by isotropic etching of silicon by an SF_6 plasma. A typical cross-section of a surface channel made by this technology is displayed in Fig. 6.

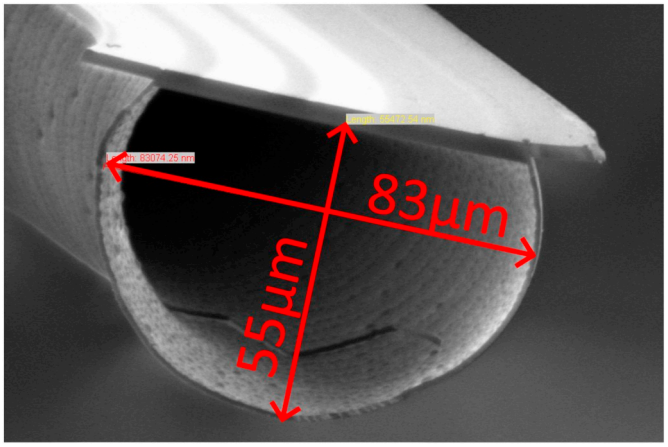

Fig. 6. Typical cross-section of a'Surface Channel' [12].

Based on simulation results, 3 types of devices were fabricated. Fig. 7 shows 3 types of devices that were fabricated. Fig. 7A shows a device with typical dimensions based on the sensor in [6]. Fig. 7B shows a device with a significantly increased channel loop size. A variation of this device with an increased in-/outlet channel length is displayed in Fig. 7C.

2.5. Measurement setup

Fig. 8 shows the measurement setup. Nitrogen gas is fed through the sensor at an input pressure of $P_{in} = 5$ while the sensor is being actuated. The mass flow is incremented in steps of 0.075 or 0.15 g/h (depending on device) from 0 to 1.2 g/h and decremented back to 0 g/h. A Polytec MSA-400 is used to measure the displacement of the channel at the measurement points indicated in Fig. 7. From these measurements, the flow sensitivity $\widehat{\Delta z_d}/\widehat{\theta_a}$ is determined for each device.

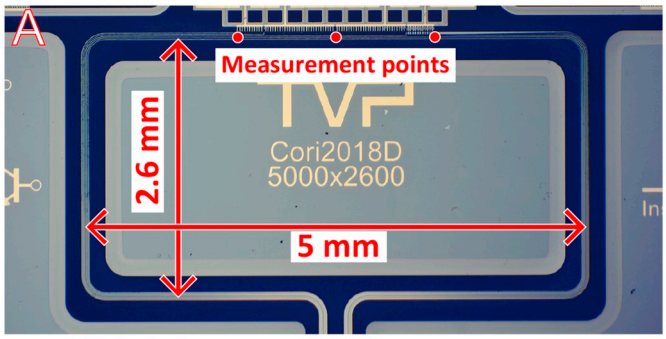

(a) Device type A with typical dimensions.

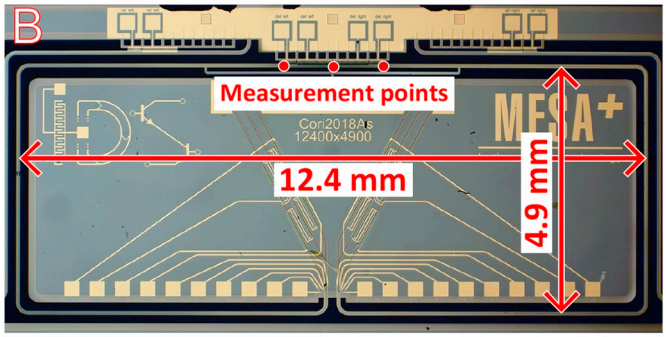

(b) Device type B with large channel loop size.

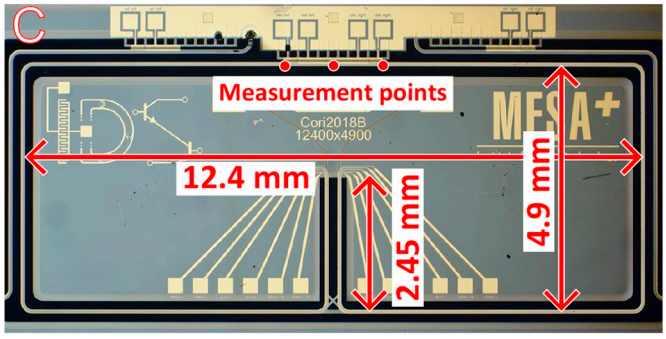

(c) Device type C with large loop size and longer in-/outlet.

Fig. 7. Microscope images of the fabricated devices. Important dimensions are indicated in the figure. Laser Doppler Vibrometer measurement points are located on the channel at the rotational axis of the actuation mode and 700 µm to the left and right of this axis.

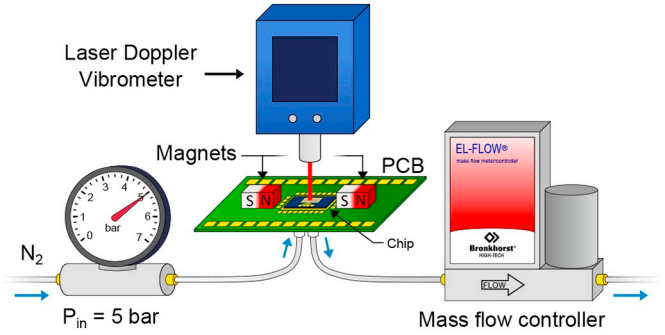

Fig. 8. Schematic representation of the measurement setup. N_2 is fed through the sensor chip with an input pressure of 5 bar (gauge pressure). A Polytec MSA-400 Laser Doppler Vibrometer is used to measure the vibrations of the μ-Coriolis.

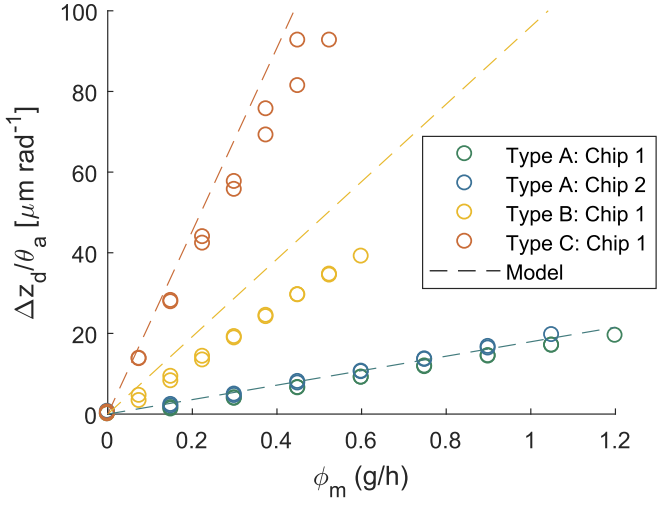

Fig. 9. Measured and modelled flow sensitivities for the devices in Fig. 7. Modelled flow sensitivities are estimated by combining output parameters of the FEM model with Eq. (16).

3. Results & discussion

Using a Polytec MSA-400 Laser Doppler Vibrometer, the ratio $\Delta z_d/\theta_a$ has been measured over a range of flows for the various devices. Fig. 9 shows the measurement results. As can be seen, the devices with a larger channel loop area have a higher flow sensitivity. This is according to Eq. (16). A longer in-/outlet length also increases sensitivity, but there is more drift in the measurement points. This is most likely due to the fact that the actuation and detection frequencies are much closer to each other in value, which makes the sensitivity more dependent on the detection mode quality factor Q_d (see Eq. (16)). Q_d changes with temperature, air pressure, humidity etc., causing the output signal to drift.

The modelled and measured parameters of the sensors are compared in Table 1. The model predicts the resonance frequencies within 10% error for all except Type A, Chip 2. There is a spread in the resonance frequencies of the fabricated devices and this device in particular is an outlier as can be seen from the table. The modelled sensitivities for type A are within 6% accurate. For Type B and C, the modelled sensitivity is predicted with approximately 20-40% error. This large error may be caused by the fact that there is a much larger pressure difference between the different sections of these large loop channel devices compared to a smaller loop device. A difference in pressure can cause a difference in stiffness of the channel sections [13]. Due to this and the fact that the density of the gas inside is also dependent on pressure, the shape of the resonance mode can also be influenced. Device B is 3.8 times more sensitive than the reference device A. Device C is 10.6 times more sensitive than Device A but shows more drift in the output signal. An optimum in-/outlet length could be found to achieve high sensitivity as well as low drift.

4. Conclusion

A model has been set up, which can determine flow sensitivity of μ-Coriolis mass flow sensors. The model was used to design new devices. These were then fabricated and characterized. Flow sensitivity of the devices has been improved approximately 4–11 times with respect to a reference device. The FEM model predicts the resonance frequencies of the devices within 10% error for all except 1 (out of 6) device(s). The predicted sensitivities are within 6–40% accurate depending on the device type. The device with the highest flow sensitivity shows significant drift in the output signal. However, the device with large channel loop area and small in-/outlet length has a high flow sensitivity and low drift. More improvements can be made upon these results with the presented model to go towards reaching the resolution of thermal flow sensors.

Declaration of competing interest

None

Table 1
Comparison of the modelled and measured parameters of the sensor devices with N_2 as flow medium. Resonance frequencies f_a and f_d are simulated in the FEM model. '-' indicates that this parameter could not be measured. *The flow sensitivity is calculated by combining the output parameters of the FEM model and Eq. (16).

		Type A			Type B	Type C	
		Chip 1	Chip 2	Chip 3	Chip 1	Chip 1	Chip 2
Actuation mode frequency f_a [Hz]	FEM Model	2602	2602	2602	576	394	394
	Measured	2382	2131	2486	544	386	398
	Error	+9.2%	+22%	+4.7%	+5.9%	+2.1%	-1.0%
Detection mode frequency f_d [Hz]	FEM Model	1593	1593	1593	359	309	309
	Measured	1491	1249	1547	350	301	306
	Error	+6.8%	+28%	+3.0%	+2.6%	+2.6%	+1.0%
Sensitivity $(\Delta z_d/\theta_a)/\phi_m$ [(μm/rad)/(g/h)]	Model*	17.9	17.9	17.9	96.1	227	227
	Measured	17.0	18.6	-	67.2	188	-
	Error	+5.3%	-3.8%	-	+43%	+21%	-

Acknowledgements

This work is part of the research programme FLOW + under project number 15019, which is co-funded by the Netherlands Organization for Scientific Research (NWO), Bronkhorst high-tech and Krohne. The authors would like to thank Jack van Putten and Jarno Groenesteijn for their help and advice during device fabrication.

References

[1] T. Wang, R. Baker, Coriolis flowmeters: a review of developments over the past 20 years, and an assessment of the state of the art and likely future directions, Flow Meas. Instrum. 40 (2014) 99–123.
[2] B.R. Binulal, J. Kochupillai, Coriolis flow meter: a review from 1989 to 2014, Int. J. Sci. Eng. Res. 5 (7) (2014) 718–723.
[3] F. Ejeian, S. Azadi, A. Razmjou, Y. Orooji, A. Kottapalli, M.E. Warkiani, M. Asadnia, Design and applications of mems flow sensors: A review, Sensors Actuators A Phys. 295 (2019) 483–502.
[4] J.T.W. Kuo, L. Yu, E. Meng, Micromachined thermal flow sensorsa review, Micromachines 3 (3) (2012) 550–573.
[5] J. Haneveld, T.S.J. Lammerink, M.J. de Boer, R.G.P. Sanders, A. Mehendale, J.C. Lötters, M. Dijkstra, R.J. Wiegerink, Modeling, design, fabrication and characterization of a micro coriolis mass flow sensor, J. Micromech. Microeng. 20 (12) (2010) 125001.
[6] J. Groenesteijn, R.G.P. Sanders, R.J. Wiegerink, J.C. Lötters, Towards nanogram per second coriolis mass flow sensing, 2016 IEEE 29th International Conference on Micro Electro Mechanical Systems (MEMS), IEEE, 2016, pp. 193–196.
[7] D. Alveringh, R.J. Wiegerink, J. Groenesteijn, R.G.P. Sanders, J.C. Lötters, Experimental analysis of thermomechanical noise in micro coriolis mass flow sensors, Sensors Actuators A Phys. 271 (2018) 212–216.
[8] D. Alveringh, J. Groenesteijn, R.J. Wiegerink, J.C. Lötters, Improved capacitive detection method for coriolis mass flow sensors enabling range/sensitivity tuning, Microelectron. Eng. 159 (2016) 1–5.
[9] A.C. de Oliveira, T.V.P. Schut, J. Groenesteijn, Q. Fan, R.J. Wiegerink, K.A.A. Makinwa, A mems coriolis mass flow sensing system with combined drive and sense interface, 2019 IEEE SENSORS, IEEE, 2019, pp. 1–4.
[10] T.V.P. Schut, Y.P. Klein, R.J. Wiegerink, J.C. Lotters, Magnetic field strength improvement for lorentz actuation of a μ-coriolis mass flow sensor, Microelectron. Eng. (2020) 111236.
[11] J. Groenesteijn, L. van de Ridder, J.C. Lötters, R.J. Wiegerink, Modelling of a micro coriolis mass flow sensor for sensitivity improvement, SENSORS, IEEE, 2014, pp. 954–957.
[12] J. Groenesteijn, M.J. de Boer, J.C. Lötters, R.J. Wiegerink, A versatile technology platform for microfluidic handling systems, part I: fabrication and functionalization, Microfluid. Nanofluid. 21 (7) (2017) 127.
[13] D. Alveringh, J. Groenesteijn, R.J. Wiegerink, J.C. Lötters, Inline pressure sensing mechanisms enabling scalable range and sensitivity, Transducers-2015 18th International Conference on Solid-State Sensors, Actuators and Microsystems (TRANSDUCERS), IEEE, 2015, pp. 1187–1190.